Pergamon

0956-7151(94)E0078-U

Acta metall. mater. Vol. 42, No. 9, pp. 3065–3070, 1994

0956-7151/94 $7.00 + 0.00

NOTCH-SENSITIVITY AND SHEAR BANDS IN BRITTLE MATRIX COMPOSITES

M.-Y. HE, B. WU and Z. SUO†

Mechanical and Environmental Engineering Department, University of California, Santa Barbara, CA 93106-5070, U.S.A.

(Received 6 October 1993; in revised form 20 January 1994)

Abstract—Matrix cracking, fiber breaking and interface sliding cause nonlinear deformation in fiber-reinforced brittle matrix composites. When a notched sample is loaded in tension, the nonlinear deformation usually localizes around the notch, spreads the stress in the ligament more evenly, and thereby leads to a higher fracture load. We simulate the interplay of two deformation mechanisms: a tensile band ahead of, and shear bands perpendicular to, a notch. The shear deformation evens out the stress distribution in the tensile band, and the strength of the tensile band sets the extent of the shear deformation. Each band is simulated by a traction–deformation law. The work of fracture is computed from a small-scale inelastic problem, and the fracture loads of notched samples from a large-scale inelastic problem. Several important conclusions emerge from the simulation. First, weak shear bands can substantially increase the work of fracture. Second, the fracture loads of notched samples are well correlated with the unnotched strength, work of fracture and notch size, by a formula independent of the shear band description. The results of the simulation are used to explain the available experimental data, and to suggest an evaluation procedure for notch-sensitivity.

1. INTRODUCTION

Compared to ductile alloys, fiber-reinforced brittle matrix composites fracture at small strains, being limited by fiber breaking strains. Yet stresses around notches in such composites can be reduced by *localized deformation*. Three deformation mechanisms have been identified [1–4]: (i) multiple matrix cracks with no fiber breaking, (ii) a tensile band consisting of broken fibers pulling out from the matrix against friction, and (iii) shear bands consisting of matrix microcracking and fiber bending. In this paper, we simulate the interplay of the tensile and the shear bands, and explore features in the results that simplify mechanical evaluation of these composites.

The simulation is motivated by recent experiments on carbon matrix composites [3, 4]. Figure 1 illustrates a notched sample loaded in tension, with shear bands extending perpendicular to the notch prior to fracture. The bands consist of microcracks in the matrix and bending of the fiber bundles. General fracture breaks the ligament ahead of the notch. Visible on a fracture surface are broken fibers and damaged matrix. For a given composite with a range of notched sample geometry and size, fracture loads are found to be well correlated by a toughness value K_c (about 15 MPa $m^{1/2}$ for a carbon matrix composite tested in [3]).

The conclusion of these experiments is better appreciated as follows. Consider a specimen containing a notch of length $2a$, which is small compared to the specimen width, subjected to remote stress $\bar{\sigma}$. Denote $\bar{\sigma}_{max}$ as the stress that causes the specimen to fracture, and evaluate the 'toughness' according to $K_c = \bar{\sigma}_{max}\sqrt{\pi a}$. Repeat the experiment for several specimens of different notch sizes. Although the fracture load $\bar{\sigma}_{max}$ decreases as the notch size increase, K_c is found to be nearly independent of the notch size. The applicability of Linear Elastic Fracture Mechanics is puzzling in this case because the specimens at the onset of fracture have large inelastic zones. In particular, the height of the shear bands often exceeds the notch size. Our simulation will resolve this paradox.

Shear bands in polymer and metal matrix composites have been modeled by various authors [5–7]. In this paper, the tensile fracture process is modeled by a traction–deformation law, Fig. 1, which is more appropriate when fiber pullout significantly contributes to fracture resistance. The near-notch shear bands do not cause fracture, but increase the tensile fracture load. The shear bands redistribute the stress in the tensile band, but do not change the bridging law.

2. THE MECHANICS MODEL

General conditions, under which composites develop near-notch shear bands, remain unclear. Shear bands are usually observed in a composite

†To whom all correspondence should be addressed.

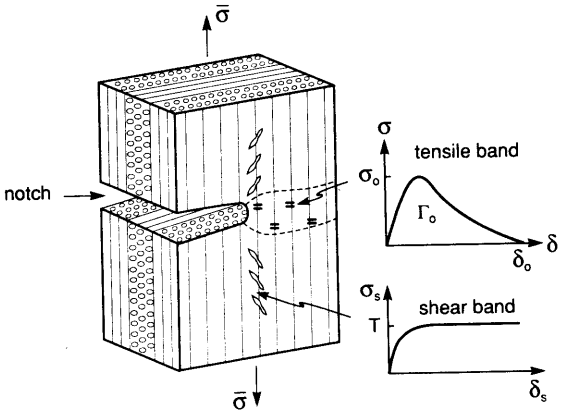

Fig. 1. A drawing of a notched sample, loaded in tension, damaged with a tensile band and two shear bands.

having higher failure strain in the matrix than in the fibers, e.g. in certain carbon, polymer and metal matrix composites. Presumably multiple matrix cracks ahead the notches are suppressed, and the shear bands set in as an alternative deformation mechanism. Depending on matrix material, either microcracking or plastic flow facilitates the shear deformation. Shear bands have been observed in unidirectional, woven and cross-ply composites.

The crack-bridging model has been applied to any composite in which the matrix fractures before the fibers. However, in composites having larger matrix failure-strains the matrix fails after the fibers. In many such materials, the complicated deformation process—fiber breaking and matrix tearing—is still localized in the vicinity of the fracture plane, and the material a small distance away from the fracture plane remains undamaged and deforms elastically. Consequently, the deformation process can still be simulated by a nonlinear traction–deformation law. In the following, the relevant results of the tensile bands without shear bands are summarized.

2.1. *Previous results on a tensile band*

A tensile band is represented by a continuous array of nonlinear springs obeying a relation between the tensile stress σ and the deformation δ

$$\sigma/\sigma_0 = \chi(\delta/\delta_0). \tag{1}$$

Here σ_0 is the bridging strength, and δ_0 the limiting deformation beyond which stress vanishes. The sample is elastic outside the band; δ is defined as the *excess deformation* in addition to the elastic deformation of the composite. The dimensionless function χ describes the shape of the curve, rising when δ is small, reaching the peak and then softening (inset of Fig. 1). The stress is assumed to be bounded everywhere in the sample, i.e. the fracture toughness at the tip of the tensile band is ignored. The simplification is justified if the crack tip toughness is small compared to the fracture resistance due to the bridging, which is usually the case for ceramic matrix composites.

The bridging law has been deduced from the propoerties of the fiber, matrix and interface for composites where matrix fractures before fibers [8, 9]. Composites having higher matrix failure-strains are less studied, but important features can be inferred. The bridging strength σ_0 must be the volume–fraction average of the matrix and fiber strengths. The fiber strength dispersion and the interface sliding resistance [10, 11] remains to be important, because they govern the thickness of the deformation band, which in turn governs the limiting deformation δ_0. In this paper, relation (1) is prescribed as a part of the constitutive description of the material.

Consider an unnotched sample subjected to a deformation-controlled load. The sample is simulated by two blocks connected by an array of springs that represent the tensile band. The two blocks deform elastically, and the springs deform uniformly according to (1). The peak load is reached at σ_0. After the peak load, the band continues to deform as the two blocks elastically unload. The sample fractures when δ reaches δ_0, and the stress vanishes everywhere. During such a stress history, the two elastic blocks return to their original states, so that the work by the external load up to fracture is solely consumed by the tensile band. Thus, the work per unit area of the tensile band is

$$\Gamma_0 = \int_0^{\delta_0} \sigma \, \mathrm{d}\delta = \sigma_0 \delta_0 \int_0^1 \chi(\xi) \, \mathrm{d}\xi. \tag{2}$$

This *work of fracture* of the springs scales with both the bridging strength and the limiting separation.

Next consider an infinite sample containing a semi-infinite notch. The two blocks are now connected by the nonlinear springs ahead of the notch, but the notch faces are free of traction. Remote from the notch tip and the tensile band, the stress field is unaffected by the nonlinear springs, and is therefore identical to the stress field around a sharp crack tip in a purely elastic block. That is, the remote stress field scales as $r^{-1/2}$, with r being the distance from the notch tip. The amplitude of the remote stress field is given by the stress intensity factor K. Of course, the stress field near the notch tip is nonsingular. The energy released when the notch extends a unit distance is given by Γ_0 [12], and the critical K_c for fracture is related to Γ_0 by $\Gamma_0 = K_c^2/E$. Here E is Young's modulus of the elastic blocks, assuming, for simplicity, that the blocks are isotropic.

Now consider an infinite sample containing a finite notch of length $2a$, subjected to remote stress $\bar{\sigma}$; see Fig. 2, the inset at the upper right corner. If the notch size is sufficiently large, an annulus exists around the notch tip, inside which the stress field is still approximately the same as the K-field. In this case, the stress intensity factor can be computed from the applied stress by the classical formula $K = \bar{\sigma}\sqrt{\pi a}$. The fracture load, $\bar{\sigma}_{\max}$, is reached when $K = K_c$.

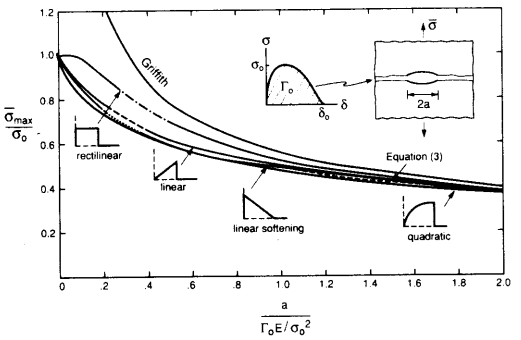

Fig. 2. Notch-sensitivity diagram.

Consequently, for a sufficiently large notch, the fracture load is given by $\bar{\sigma}_{\max} = (\Gamma_0 E/\pi a)^{1/2}$. This is the Griffith condition plotted in Fig. 2.

When the notch is small, nowhere in the two blocks can the stress field be the same as the K-field. As such, the stress intensity factor cannot be defined for two blocks connected by springs with a small notch. Yet the fracture load can be computed as follows. When subjected to the stress $\bar{\sigma}$, the two blocks separate more at the tip of the notch than at a position ahead of the notch tip. This nonuniformity causes the notched sample to fracture at a stress $\bar{\sigma}$ below the bridging strength σ_0. Analyzing the problem coupling the elastic blocks and the nonlinear springs, one determines the applied stress $\bar{\sigma}$ as a function of the separation at the notch tip δ_t. For the generic bridging law shape in Fig. 2, the applied stress $\bar{\sigma}$ first increases with the notch tip separation δ_t, reaches a peak $\bar{\sigma}_{\max}$, and then drops. This peak stress is the fracture load.

Figure 2, referred to as a *notch-sensitivity diagram*, summarizes the calculated fracture loads for several bridging law shapes [13, 14]. For each bridging law shape, the peak stress is σ_0, the limiting displacement is δ_0, and the work of fracture Γ_0 is the area under the bridging law as given by (1). Each bridging law defines a basic *material length* $\Gamma_0 E/\sigma_0^2$ which, roughly speaking, scales the size of the zone where the nonlinearity is important. The notch size a is measured in units of this material length in Fig. 2. As evident from the diagram, the results do not vary significantly with the bridging law shapes. As discussed before, the Griffith condition is the exact asymptote for large notches, but incorrect for small notches. Independent of the bridging law shape χ, the same limit is approached at each end of the diagram: the fracture load approaches the unnotched strength $\bar{\sigma}_{\max} = \sigma_0$ when the notch size is small, and is given by the Griffith formula when the notch is large. Accordingly, it is not surprising that different bridging laws give similar results.

The following formula interpolated from the two limits gives the approximate fracture loads for any finite notch size

$$\bar{\sigma}_{\max}/\sigma_0 = [1 + \pi a/(\Gamma_0 E/\sigma_0^2)]^{-1/2}. \tag{3}$$

This equation is also included in Fig. 2. Given a composite with a fixed material length $\Gamma_0 E/\sigma_0^2$, the fracture load will not be significantly reduced by the presence of a notch provided the notch size is small, say $a/(\Gamma_0 E/\sigma_0^2) < 0.1$. On the other hand, the Griffith formula is approximately valid when $a/(\Gamma_0 E/\sigma_0^2) > 2$.

2.2. *Simultaneous tensile and shear bands*

In what follows we investigate the interaction between the tensile and the shear bands. Since the shape of the bridging law is of secondary importance, we will study this interaction by assuming that the tensile band deforms like an array of linear springs:

$$\sigma = k\delta. \tag{4}$$

Here k is the spring stiffness and, as before, the spring breaks at stress σ_0. The work of fracture of an unnotched sample with a uniformly deforming tensile band is

$$\Gamma_0 = \sigma_0^2/2k. \tag{5}$$

We will assume that the stress is bounded everywhere; that is, the stress intensity factor vanishes at the tip tensile band. For the linear spring model, this implies that the tensile band spreads over the entire ligament ahead of the notch.

The interaction between the tensile and the shear bands can be understood as follows. The separation of the tensile band is nonuniform near a notch. With the linear law used in this simulation, the sample fractures when the stress at the tail of the tensile band reaches σ_0. At this point, the stress at the other positions in the tensile band is below σ_0, so that the failure load is less than the net cross-section times σ_0. The shear bands will make the separation of the tensile band less nonuniform, and thereby give rise to higher fracture loads. On the other hand, the extent of the shear bands is governed by the strength of the tensile band. For example, in the limiting case when the tensile band is vanishingly weak, the shear band will not form before the composite breaks.

To assess the general validity of certain conclusions, two descriptions of the shear bands will be used in this paper. In the first description, Fig. 3(a), the shear stress σ_s and the sliding displacement δ_s are connected by

$$\sigma_s = k_s \delta_s. \tag{6}$$

The spring stiffness k_s is a material constant. The stress intensity is assumed to vanish at the tips of the shear bands. For the linear spring model, this requires that the shear bands extend to the sample boundary, Fig. 3(a).

Shear experiments with a carbon matrix composite show that a constant resistance prevails over almost the entire shear deformation process [4]. This will

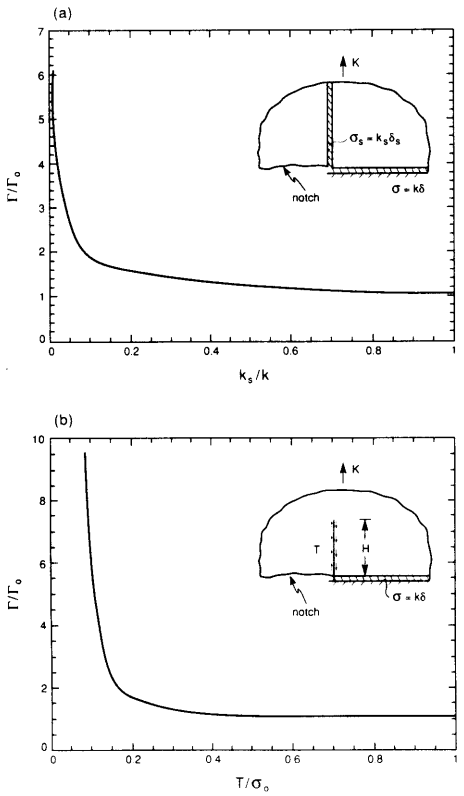

Fig. 3. Fracture energy ratios showing the contribution of the shear bands: (a) shear band is an array of linear springs, and (b) shear band has a constant resistance T.

be used as a second description in the simulation, i.e. a constant shear resistance T is prescribed in the shear bands, Fig. 3(b). It is assumed that T is a material property invariant with sample size and geometry. For this description, the vanishing stress intensity at the tips of the shear bands will determine a finite height of the bands, H, Fig. 3(b).

As before, the elastic response of the composites is taken to be isotropic. The shear bands are assumed to remain closed, so that the normal displacements are continuous across the shear bands. All numerical calculations were done with the ABAQUS finite element code, under plane stress conditions, with Poisson's ratio $\nu = 0.3$. This solution is also applicable to plane strain conditions if Young's modulus E everywhere is replaced by $E/(1-\nu^2)$.

3. RESULTS

3.1. Work of fracture

Figure 3 shows a semi-infinite notch in an infinite sample. The stress field remote from the notch tip is prescribed by the square-root singular solution, scaled with the intensity factor K. The fracture toughness K_c is attained when the stress at the tail of the tensile band σ_t reaches the spring strength σ_0. Once K_c is computed, the work of fracture of the composite (as opposed to that of the springs) is computed from

$$\Gamma = K_c^2/E. \tag{7}$$

The ratio Γ/Γ_0 indicates the role of the shear bands in toughening the composites.

First use the description that the shear bands behave like linear springs. Linearity and dimensional considerations dictate that

$$\sigma_t = \alpha K(k/E)^{1/2}. \tag{8}$$

The dimensionless number α depends only on k_s/k, which is computed using finite elements. In the above, $K = K_c$ when $\sigma_t = \sigma_0$. A combination of (5), (7) and (8) gives

$$\Gamma/\Gamma_0 = 2/\alpha^2. \tag{9}$$

Figure 3(a) plots the calculated results. As anticipated, stiff shear bands add little to the work of fracture, but weak shear bands add substantially.

Next use the description that the shear deformation is resisted by a constant stress T. The system is linear in both K and T so that

$$\sigma_t = f_1 KH^{-1/2} + f_2 T, \tag{10}$$

$$K_{II} = f_3 K - f_4 TH^{1/2}. \tag{11}$$

Here K_{II} is the mode II stress intensity factor at the tip of the shear band, and fs are dimensionless numbers depending in Hk/E. With $K_{II} = 0$ and $\sigma_t = \sigma_0$, one rearranges (10) and (11) as

$$T/\sigma_0 = 1/(f_2 + f_1 f_4/f_3), \tag{12}$$

$$\Gamma/\Gamma_0 = 2(Hk/E)/(f_1 + f_2 f_3/f_4)^2. \tag{13}$$

Once the coefficients f_i are computed by using finite elements, the above defines a relation between Γ/Γ_0 and T/σ_0 via the parameter Hk/E. This relation is plotted in Fig. 3(b). Again, the shear bands contribute little to the work of fracture if the shear resistance T is large.

That the curves in Fig. 3(a, b) turn sharply may be an artifact due to the model used in this paper. In reality, the inelastic deformation is not localized to the mathematical planes. In some composites, the shear bands may involve more intricate micromechanisms, which cannot be described by a simple traction law [5]. These uncertainties will persist in any model that predicts work of fracture. However, the situation becomes much better when one tries to correlate the fracture loads of notched samples with an *experimentally measured* work of fracture, as demonstrated in the following.

3.2. Notch-sensitivity

Consider a sample containing a finite notch loaded in tension by stress $\bar{\sigma}$, Fig. 4(a). The notch size $2a$ is small compared to the sample width, so that the sample is assumed to be infinite. The fracture loads in the absence of the shear bands are given in Fig. 2; the enhancement due to the shear bands is

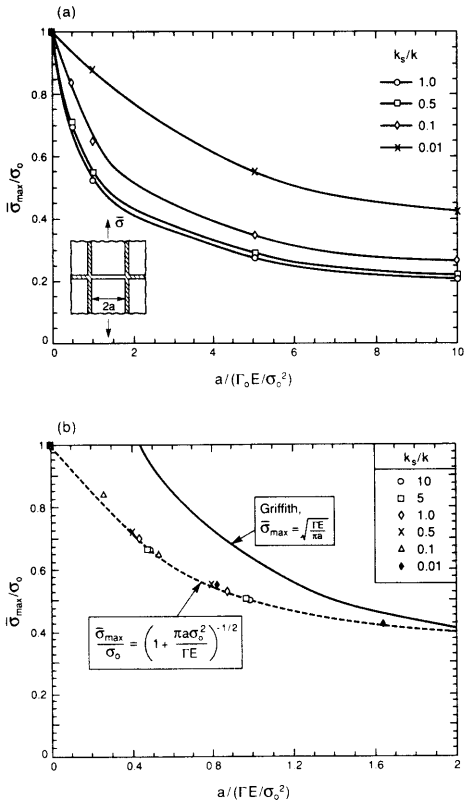

Fig. 4. Notch-sensitivity diagram including shear bands with linear stress-sliding law. (a) The notch size is normalized by the work of fracture of the tensile band, Γ_0. (b) The crack size is normalized by the total work of fracture, Γ.

studied in this section. For composites with the linear stress–deformation laws (4) and (6), both tensile and shear bands extend to the sample boundary. The stress in the tail of the tensile band varies linearly with the applied stress:

$$\sigma_t = \beta\bar{\sigma}. \tag{14}$$

Here β depends on both k_s/k and ak/E, which is computed using finite elements. Note that $ak/E = a/(2\Gamma_0 E/\sigma_0^2)$ for the linear spring. For the linear spring, the applied stress $\bar{\sigma}$ reaches the fracture load, $\bar{\sigma}_{max}$, when σ_t reaches the bridging strength σ_0. Consequently, $\bar{\sigma}_{max}/\sigma_0 = 1/\beta$, which is plotted in Fig. 4(a). The fracture loads depend on shear property k_s/k. Weak shear bands relieve stress concentration and thereby lead to high fracture loads. The diagram conveys the essentials of the role of the shear bands, but is difficult to use in practice because of the uncertainties in the shear band characterization discussed previously.

Figure 4(b) plots the same results, but using the total work of fracture Γ of semi-infinite notches calculated previously to replace Γ_0. The new diagram shows that curves for different values of k_s/k collapse onto one curve. That is, the fracture loads are insensitive to the constitutive details of the shear bands, so long as the total work of fracture Γ is used to scale the diagram. The outcome is not unexpected because, again, the curves for different values of k_s/k have the same asymptote for either small or large notches. For small notches, the fracture load is close to the strength of the unnotched composite, $\bar{\sigma}_{max} = \sigma_0$. For large notch, the fracture load is given by Griffith formula, $\bar{\sigma}_{max} = (\Gamma E/\pi a)^{1/2}$. Indeed, the fracture load curve in Fig. 4(b) is identical to that in Fig. 2 computed using the linear springs.

Encouraged by this finding, we then use constant T for the shear bands to confirm the general validity [Fig. 5(a)]. The tensile stress at the notch tip and K_{II} at the shear band tip are linear in $\bar{\sigma}$ and T:

$$\sigma_t = g_1\bar{\sigma} + g_2 T, \tag{15}$$

$$K_{II}H^{-1/2} = g_3\bar{\sigma} - g_4 T. \tag{16}$$

The dimensionless coefficients g_i depend on ak/E and Hk/E, and were calculated by using finite elements. With $K_{II} = 0$ and $\sigma_t = \sigma_0$, one finds from (15) and (16) that

$$T/\sigma_0 = 1/(g_2 + g_1 g_4/g_3), \tag{17}$$

$$\bar{\sigma}_{max}/\sigma_0 = 1/(g_1 + g_2 g_3/g_4). \tag{18}$$

For a given notched composite, ak/E and T/σ_0 are fixed, the shear band height H at the onset of fracture is determined from (17). Using this height, one can plot (18) in the form of Fig. 5(a). The fracture loads vary with shear resistance T, as anticipated. The same results are plotted in Fig. 5(b), replacing Γ_0 by Γ computed previously. Once again, the notch-sensitivity diagram is almost independent of the shear

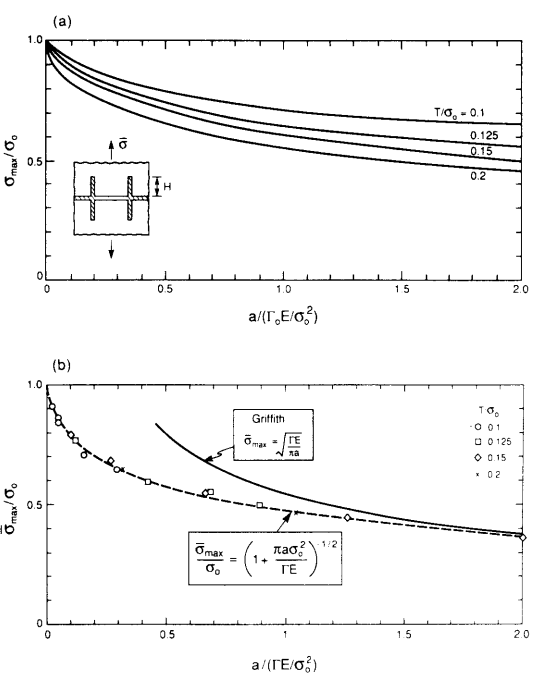

Fig. 5. Notch-sensitivity diagram including shear bands with constant resistance. (a) The notch size is normalized by the work of fracture of the tensile band, Γ_0. (b) The crack size is normalized by the total work of fracture, Γ.

band property T/σ_0. For small T/σ_0, our calculations have shown that the height of the shear bands H can be several times the notch size a at the onset of fracture.

Note that the fracture load curves in Figs 4(b) and 5(b) are identical, even though the shear properties are different. Given the uncertainties in characterizing nonlinear deformation near the notches, a pragmatic approach to determine fracture loads in notched samples should be valuable. As suggested by the present simulation, two meausurements are required for a given composite: the bridging-strength σ_0 from an unnotched sample, and the work of fracture Γ from a sample containing a "large" notch. The latter may be readily accomplished in practice because the Griffith formula $\bar{\sigma}_{max} = (\Gamma E/\pi a)^{1/2}$ is valid so long as $a/(\Gamma E/\sigma_0^2) > 2$. This condition applies even when the height of the shear bands is larger than the notch size. The fracture loads for a sample containing a finite notch can then be obtained from Fig. 2 or equation (3), with Γ_0 replaced by the measured Γ.

An example using the experimental data in [3] will illustrate the procedure. For a carbon–carbon composite, the unnotched strength is measured to be $\sigma_0 = 300$ MPa, the fracture load is $\bar{\sigma}_{max} = 100$ MPa for a sample with notch size $a = 6$ mm. Upon fracture, the height of the shear band is slightly larger than the notch size. Using the standard calibration for a crack in an infinite sample, one finds that the fracture toughness is $K_c = \bar{\sigma}_{max}\sqrt{\pi a} = 14$ MPa m$^{1/2}$. (The finite sample width only gives a small correction.) Also note that $a/(\Gamma E/\sigma_0^2) = a/(K_c/\sigma_0)^2 = 2.4$, so that the notch is large enough for the Linear Fracture Mechanics to apply. The fracture loads measured from samples containing notches of $a = 1, 2, 4, 6$ mm indeed are well represented by the notch sensitivity diagram; see Fig. 5(a) in [3].

4. CONCLUDING REMARKS

Three important conclusions are drawn from this simulation. First, shear bands in brittle–matrix composites can substantially increase work of fracture, which in turn reduces notch-sensitivity. Second, regardless of the relative height of the shear bands H/a, Linear Fracture Mechanics is valid if the notch size is sufficiently large, $a/(K_c/\sigma_0)^2 > 2$. Third, for samples containing small notches, the fracture loads are well correlated with the work of fracture, the unnotched strength and the notch size by

$$\bar{\sigma}_{max}/\sigma_0 = [1 + \pi a(\sigma_0/K_c)^2]^{-1/2}.$$

Note that the formula is independent of the shear band properties and the relative height H/a, but is restricted to samples having small notches compared to the width. The conclusions are reached by two shear band descriptions with wide range parameter variations, and are expected to have much more general validity. For example, finite samples with either crack-like notches or holes may be similarly treated. That is, the notch sensitivity diagrams presented in [13] can be used with materials with shear bands, with Γ reinterpreted as the total work of fracture.

Acknowledgements—The authors wish to thank Professor B. Budiansky for reviewing the manuscript and suggesting improvements. The work was supported by the Defense Advanced Research Projects Agency through the University Research Initiative under the Office of Naval Research contract N-0014-92-J-1808. Z. Suo was also supported by the National Science Foundation through a Young Investigator Award MSS-9258115.

REFERENCES

1. C. Cady and A. G. Evans, *J. Am. Ceram. Soc.* In press.
2. J. M. Domergue, H. C. Cao, A. G. Evans and D. Petrak, *J. Am. Ceram. Soc.* In press.
3. F. E. Heredia, S. M. Spearing, T. J. Mackin, M. Y. He, A. G. Evans, P. Mosher and P. Brondsted, *J. Am. Ceram. Soc.* In press.
4. P. Brondsted, F. E. Heredia and A. G. Evans, *J. Am. Ceram. Soc.* In press.
5. M. Spearing, P. W. R. Beaumont and M. F. Ashby, in *Composite Materials: Fatigue and Fracture*, (edited by T. K. O'Brien), p. 596. ASTM STP 1110 (1991).
6. Y. A. Bahei-El-Din, G. J. Dvorak and J.-F. Wu, *Engng Fract. Mech.* **34,** 105 (1989).
7. J. Tirosh, *J. appl. Mech.* **40,** 785 (1973).
8. D. B. Marshall, B. N. Cox and A. G. Evans, *Acta metall. mater.* **35,** 2607 (1985).
9. D. B. Marshall, M. C. Shaw and M. L. Morris, *Acta metall. mater.* **40,** 443 (1992).
10. M. D. Thouless and A. G. Evans, *Acta metall.* **36,** 517 (1988).
11. W. A. Curtin, *J. Mech. Phys. Solids* **41,** 217 (1993).
12. J. R. Rice, *ASME J. appl. Mech.* **35,** 379 (1968).
13. Z. Suo, S. Ho and X. Gong, *ASME J. Engng Mater. Tech.* **115,** 319 (1993).
14. B. Budiansky and Y. L. Cui, *J. Mech. Phys. Solids.* **42,** 1 (1994).